J. Phys. B: Atom. Molec. Phys., Vol. 10, No. 9, 1977. Printed in Great Britain.

Application of the Baylis–Gombas pseudopotential to inelastic atomic collisions

Karna J Wahlstrand†§, Robert W Numrich†‖, John S Dahler† and Svend Erik Nielsen‡

† Department of Chemistry, University of Minnesota, Minneapolis, Minnesota 55455, USA

‡ Chemistry Laboratory III, H C Ørsted Institute, University of Copenhagen, DK-2100, Copenhagen Ø, Denmark

Received 17 November 1976

Abstract. Calculations are reported of matrix elements of the Baylis–Gombas model potential for Li–He and Li–Ne interactions. Included are comparisons of two computational approaches, one based upon a numerical double-integration procedure, the other an analytical, approximative method. The special emphasis of the calculation is the sensitivity of matrix elements that are important for collision-induced electronic transitions to the pecise choice of the Baylis model parameter r_0. Also reported and compared to the Baylis results are calculations of Li–He/Ne matrix elements for a Hartree–Fock frozen-core model potential and for two Bottcher-type model potentials. Applications of the different models to the prediction of inelastic collision cross sections are reported in an accompanying paper.

1. Introduction

The information presented here is part of a systematic study we are conducting of high-energy atomic collisions involving excitation, exchange and detachment of outer-shell valence electrons. Key elements in the interpretation and theoretical analysis of these events are the effective forces exerted on the valence electron(s) by the two atomic cores. Hartree–Fock fields and the model potentials developed by Bottcher (1971) and Bottcher *et al* (1973) are two approximations one can use for this purpose. Another is the model proposed by Baylis (1969) for the purpose of calculating interatomic potentials of ground and low-lying excited states of diatomic systems composed of an alkali atom and a ground-state rare-gas atom. Our intention is to use the one-electron Hamiltonian generated by this procedure as a model for calculating cross sections of various collision-induced electronic transitions.

The present paper includes a brief description of the Baylis model and an outline of the computational procedure we have used to evaluate matrix elements of the corresponding approximation to the effective potential. Also reported here are calculations which illustrate how sensitively these matrix elements depend upon the model parameters and how these elements compare with results based on Hartree–Fock

§ Present address, Department of Chemistry, Harvard University, Cambridge, Massachusetts, USA.

‖ Present address, Department of Chemistry, Kansas State University, Manhattan, Kansas, USA.

and Bottcher potentials. In the following paper (Manique *et al* 1977) excitation cross sections calculated from these Baylis matrix elements are compared with cross sections derived from the other two models. Further studies involving different applications of these same matrix elements are in progress and will be reported separately.

1.1. Baylis model

We consider the interaction between an alkali atom, A, with one valence electron and $Z_A - 1$ core electrons, and a rare-gas atom, B, with Z_B core electrons. The vectors extending from one nucleus to the other and from the two nuclei to the valence

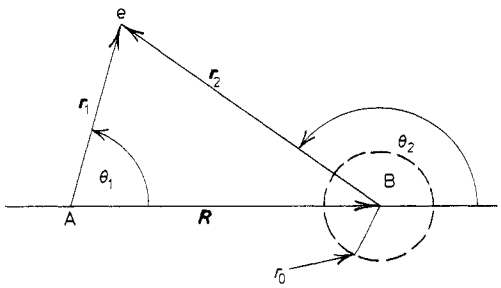

Figure 1. Coordinates used to describe the relative positions of the alkali ion A^+, the rare-gas atom B, and the valence electron e^-. The rare-gas atom has a 'core' radius r_0.

electron are denoted by the symbols $\overrightarrow{AB} = \boldsymbol{R}$, $\overrightarrow{Ae} = \boldsymbol{r}_1$ and $\overrightarrow{Be} = \boldsymbol{r}_2$ and are depicted in figure 1. The tightly bound cores of the two atoms are represented by unperturbed wavefunctions. This approximation certainly is valid if the collision energy is much less than the core excitation energies and it also should be reasonable at much larger energies provided that one is concerned exclusively with processes which directly involve only the valence electron. To this approximation the system can be treated as if it consisted of three 'particles', the valence electron and the cores of the two atoms. According to the Baylis model the potential energy operator of this three-body system (chosen to be zero when the three particles are infinitely far apart) is the sum, $V_A(r_1) + V_I(\boldsymbol{r}_2, \boldsymbol{R})$, of local potential energy functions. Here $V_A(r_1)$ is the interaction between the valence electron and the unperturbed core of the alkali atom. The remainder of the interaction energy is separated into three parts:

$$V_I(\boldsymbol{r}_2, \boldsymbol{R}) = F(\boldsymbol{r}_2, \boldsymbol{R}) + G(r_2) + W(R). \tag{1}$$

The first of these contributions is the electrostatic interaction computed as if the alkali atom were two point charges—one with charge $+e$ located at the alkali nucleus and another with charge $-e$ fixed at the position of the valence electron—and as if the rare-gas atom were a polarizable charge distribution with radius r_0 and polarizability α_B. Thus,†

$$F(\boldsymbol{r}_2, \boldsymbol{R}) = -\tfrac{1}{2}\alpha_B[\boldsymbol{E}(\boldsymbol{r}_2, \boldsymbol{R})]^2 \tag{2}$$

where $\boldsymbol{E}(\boldsymbol{r}_2, \boldsymbol{R}) = -(\boldsymbol{R}/R^3 + \boldsymbol{r}_2/r_2^3)$ is the value of the (dipole) electric field vector at the nucleus of the rare-gas atom. When r_2 is less than r_0, E^2 is replaced with its average over the surface of a sphere of radius r_0 centred at $\boldsymbol{R}$, the location of the

† Atomic units ($e = m_e = \hbar = 1$) are used throughout this paper.

rare-gas atom B. Therefore,

$$E^2 = \begin{cases} \dfrac{1}{R^4} + \dfrac{1}{r_2^4} + \dfrac{2}{R^2 r_2^2}\cos\theta_2 & r_2 \geqslant r_0 \\ \dfrac{1}{R^4} + \dfrac{1}{r_0^4} & r_2 < r_0 \end{cases} \tag{3}$$

where the angle $\theta_2 = \cos^{-1}(\hat{\boldsymbol{R}}.\hat{\boldsymbol{r}}_2)$ is as illustrated in figure 1.

The functions G and W are the Gombas-type pseudopotentials

$$G(r_2) = \tfrac{1}{2}[3\pi^2\rho_B(r_2)]^{2/3} \tag{4}$$

and

$$W(R) = \tfrac{3}{10}(3\pi^2)^{2/3}\int d^3r_1\{[\rho_A(r_1) + \rho_B(r_2)]^{5/3} - \rho_A^{5/3}(r_1) - \rho_B^{5/3}(r_2)\} \tag{5}$$

based upon the Thomas–Fermi statistical model of atoms. Here $\rho_B(r_2)$ denotes the density of the rare-gas electron distribution at a distance r_2 from the point B and $\rho_A(r_1)$ is the analogous density function associated with the core electrons of the alkali atom. For the densities of these cores Baylis (and we too) used SCF expressions of the form (Clementi 1965)

$$\rho(r) = \frac{1}{4\pi}\sum_s \zeta(s) r^{\alpha(s)} \exp[-2\beta(s)r] \tag{6}$$

with the sum extending over all closed shells. Here $\zeta(s)$ is a normalization factor and $\alpha(s)$ and $\beta(s)$ are variationally determined parameters.

Aside from these coefficients, the only parameters that appear in the model potentials are the 'radii', r_0, of the rare-gas atoms. The values of these radii are determined by fitting the depths of the ground-state potentials of the AB systems to those obtained from experiments. The same experimental data and the same techniques for performing these determinations have been used by Baylis (1969) and by Pascale and Vandeplanque (1974). However, because they used different basis sets to diagonalize the one-electron operator, $\hat{H} = -\frac{1}{2}\nabla^2 + V_A(r_1) + V_I(\boldsymbol{r}_2, \boldsymbol{R})$, and hence to calculate the adiabatic potential energies of the AB system, the r_0 values generated by these two investigators were not the same. Furthermore, in most cases (helium being a notable example to the contrary) the calculated values of the well depths are not especially sensitive to the values of r_0. Because of this it is imperative for us to establish how sensitively the matrix elements and cross sections we calculate depend upon the (uncertain) values of the radii r_0.

To diagonalize $\hat{H}$ both Baylis and Pascale and Vandeplanque used approximate, alkali valence-electron wavefunctions of the Bates–Damgaard type. These differ somewhat (especially near the nucleus) from the exact eigenfunctions of $\hat{H}_A = -\frac{1}{2}\nabla^2 + V_A(r_1)$ that were used in our calculations and which are described immediately below. However, we do not believe that this produces inconsistencies of any importance.

1.2. Alkali-atom valence-electron wavefunctions

For the valence electron of the alkali atom we use the orbitals $\phi^A_{nlm}(\boldsymbol{r}) = Y_{lm}(\hat{r})\mathscr{R}_{nl}(r)$ where the radial functions $\mathscr{R}_{nl}(r)$ have been obtained from the exact numerical solution

of the one-dimensional eigenvalue problem associated with the operator $\hat{H}_A$. These eigenfunctions were fitted to expressions of the form,

$$\mathscr{R}_i(r) = N_i \mathscr{P}_i(r) \mathscr{E}_i(r)$$

where $\mathscr{P}_i(r)$ is a polynomial and

$$\mathscr{E}_i(r) = \exp(-f_i r) + g_i \exp(-h_i r).$$

In the cases of sodium and the heavier alkali metals the numerical solutions are fitted somewhat better if g_i is replaced with $g_i(r - r_i)$. This procedure has been described by Rapp and Chang (1972, 1973).

2. Matrix elements of the Baylis potential

What we wish to evaluate are the matrix elements,

$$V_{jj'}(\boldsymbol{R}) = (\phi^A_{nlm}|V_1|\phi^A_{n'l'm'}) = \int d^3 r_1 \mathscr{R}_{nl}(r_1) \mathscr{R}_{n'l'}(r_1) \bar{Y}_{lm}(\hat{r}_1) Y_{l'm'}(\hat{r}_1) V_1(\boldsymbol{r}_2, \boldsymbol{R}), \tag{7}$$

of the potential energy operator

$$V_1 = F + G + W \equiv U_1 + W. \tag{8}$$

Here the spherical harmonics and their arguments may be referred either to the laboratory frame of reference or to the body-fixed rotating frame with polar axis parallel to $\boldsymbol{R}$. In either case $V_{jj'} = \delta(j|j')W(R) + U_{jj'}$ where $U_{jj'}$ denotes a matrix element of the operator $U_1 = F + G$.

Matrix elements in the lab and body-fixed frames are related by

$$U^{(\mathrm{LAB})}_{nlm,n'l'm'}(\boldsymbol{R}) = \sum_{\mu,\mu'} R^{(l)}_{m\mu}(\hat{R}) \bar{R}^{(l')}_{m'\mu'}(\hat{R}) U^{(\mathrm{BODY})}_{nl\mu,n'l'\mu'}(R) \tag{9}$$

where the $R^{(l)}$ denote representation coefficients of the rotation group (Messiah 1962). Because of the (AB) axial symmetry of $U_1(r_2, \boldsymbol{R})$ [$= U_1(r_1, r_2, R)$], the body-fixed matrix elements of this operator are diagonal with respect to the projection (magnetic) quantum numbers.

2.1. Numerical integration procedure

To evaluate the matrix elements $U^{(\mathrm{BODY})}_{jj'}(R)$ we introduce the elliptic coordinates $\lambda = R^{-1}(r_1 + r_2)$ and $\mu = R^{-1}(r_1 - r_2)$, with the ranges $1 \leqslant \lambda \leqslant +\infty$ and $-1 \leqslant \mu \leqslant 1$, respectively. A 32-point Gauss–Legendre formula was used for the μ integration and a 48-point formula for λ. Points were distributed over the ranges of integration by the technique of McLean and Yoshimine (1965). The numerical integration method was adapted from a program due to Schaefer (1970).

The only problem is with the discontinuity of $F(\boldsymbol{r}_2, \boldsymbol{R})$ on the sphere $r_2 = r_0$. In elliptic coordinates the equation of this sphere is $\lambda - \mu = 2r_0/R$. When $r_0 < R$ the interior of this sphere corresponds to the triangular region labelled I in figure 2(*a*). When $r_0 > R$ the interior region, $r_2 < r_0$, corresponds to the trapezoidal region, I, of figure 2(*b*). From this figure we see that the representative integral

$$J = \int_0^\infty dr_1 r_1^2 \int_0^\pi d\theta_1 \sin\theta_1 J(r_1, \theta_1) = \int_{-1}^1 d\mu \int_1^\infty d\lambda \mathscr{J}(\lambda, \mu),$$

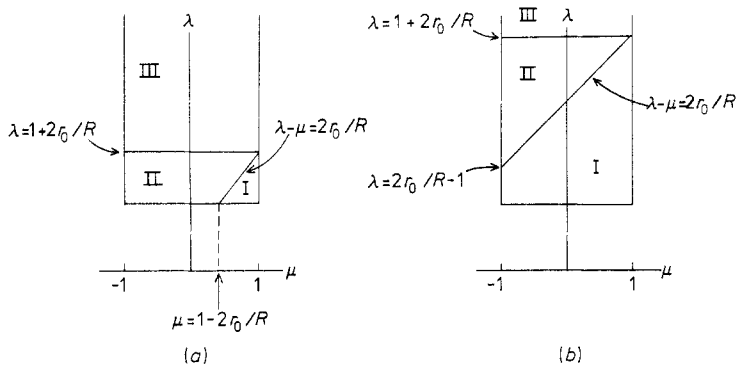

Figure 2. Regions of integration involved in the double-integration procedure. (*a*) $r_0 < R$; (*b*) $r_0 > R$.

with $\mathcal{J}(\lambda, \mu) = (R/2)^3(\lambda^2 - \mu^2)J(r_1, \theta_1)$, can be written as the sum of three contributions

$$J_{\mathrm{I}} = \int_a^1 \mathrm{d}\mu \int_1^{\mu + 2r_0/R} \mathrm{d}\lambda \mathcal{J}(\lambda, \mu)$$

$$J_{\mathrm{II}} = \int_b^{1 + 2r_0/R} \mathrm{d}\lambda \int_{-1}^{\lambda - 2r_0/R} \mathrm{d}\mu \mathcal{J}(\lambda, \mu)$$

and

$$J_{\mathrm{III}} = \int_{-1}^1 \mathrm{d}\mu \int_{1 + 2r_0/R}^{\infty} \mathrm{d}\lambda \mathcal{J}(\lambda, \mu),$$

one associated with each part of the integration range. Here, $a = \max(-1, 1 - 2r_0/R)$ and $b = \max(1, 2r_0/R - 1)$.

This subdivision of the integration range is needed only for the integrals involving the discontinuous integrand function $F(r_2, \boldsymbol{R})$. However, once the integration grid has been set up, it takes very little extra time to calculate the G and W matrix elements in the same way. This is the procedure we have used. It was tested by evaluating known integrals.

The method of McLean and Yoshimine allows one to vary the distribution of points (on the integration grids over the three regions) by specifying a few parameter values. Variations of these parameters did not alter our results to at least ten significant figures.

2.2. Analytic evaluation of matrix elements

It is possible to avoid the double integration procedure outlined above by evaluating the matrix elements analytically. To illustrate how this can be done we begin with the easily derived formula

$$U^{(\mathrm{BODY})}_{nlm,n'l'm'}(R) = 2\pi \sum_L \mathrm{a}_L(nlm, n'l'm')B^L(nl, n'l'|R) \tag{10}$$

where

$$a_L(nlm, n'l'm') = \delta_{mm'}(-1)^m \left(\frac{(2l + 1)(2l' + 1)}{4\pi(2L + 1)}\right)^{1/2} \langle ll'00|L0\rangle \langle ll' - mm|L0\rangle \tag{11}$$

and

$$B^L(nl, n'l'|R) = \frac{1}{R}\int_0^\infty dr_2 r_2 \int_{|r_2-R|}^{r_2+R} dr_1 r_1 \mathscr{R}_{nl}(r_1)\mathscr{R}_{n'l'}(r_1) Y_{L0}(\theta_1, 0) U_1(r_1, r_2, R). \tag{12}$$

In terms of these same functions the lab-frame matrix elements are given by

$$U^{(\mathrm{LAB})}_{nlm,n'l'm'}(\boldsymbol{R}) = 2\pi(-1)^m \sum_L \frac{[(2l+1)(2l'+1)]^{1/2}}{2L+1} \langle ll'00|L0\rangle \langle ll' - mm'|L, m'-m\rangle$$
$$\times Y_{L,m'-m}(\hat{R}) B^L(nl, n'l'|R).$$

Let us now rewrite the electrostatic interaction in the form

$$F(\boldsymbol{r}_2, \boldsymbol{R}) = r_1 \cos\theta_1 \, U_1(r_2, R) + U_2(r_2, R)$$

where

$$U_1(r_2, R) = \begin{cases} -\alpha_B \dfrac{1}{R^2 r_2^3} & r_2 \geqslant r_0 \\ 0 & r_2 < r_0 \end{cases}$$

and

$$U_2(r_2, R) = \begin{cases} -\dfrac{\alpha_B}{2}\left(\dfrac{1}{R^4} + \dfrac{1}{r_2^4} - \dfrac{2}{Rr_2^3}\right) & r_2 \geqslant r_0 \\ -\dfrac{\alpha_B}{2}\left(\dfrac{1}{R^4} + \dfrac{1}{r_0^4}\right) & r_2 < r_0. \end{cases}$$

From this it follows directly that

$$B^L(|R) = \sum_{L'}\left(\frac{2L+1}{2L'+1}\right)^{1/2} \langle 1L00|L'0\rangle^2 B^{(L',2)}_{U_1}(|R) + B^{(L,1)}_{U_2}(|R) + B^{(L,1)}_{G}(|R) \tag{13}$$

with

$$B^{(L,S)}_X(i, j|R) = \frac{1}{R}\int_0^\infty dr_2 r_2 X(r_2, R) K^{(L,S)}_{i,j}(r_2, R) \tag{14}$$

and

$$K^{(L,S)}_{i,j}(r_2, R) = \int_{|R-r_2|}^{R+r_2} dr_1 r_1^S Y_{L0}(\theta_1, 0)\mathscr{R}_i(r_1)\mathscr{R}_j(r_1). \tag{15}$$

Then from the identity $\cos\theta_1 = (r_1^2 + R^2 - r_2^2)/2r_1R$ and the polynomial representation of $P_L(\cos\theta_1)$ it can be shown that

$$K^{(L,S)}_{i,j}(r_2, R) = 2^{-L}\left(\frac{2L+1}{4\pi}\right)^{1/2} \sum_{n=0}^{[L/2]} \frac{(-1)^n(2L-2n)!}{n!(L-n)!}(2R)^{2n-L} \sum_{k=0}^{L-2n} \frac{1}{(L-2n-k)!}$$
$$\times \sum_{p=0}^{k} \frac{(-1)^p R^{2k-2p}}{p!(k-p)!} r_2^{2p} FQ^{ij}_{S+L-2n-2k}(r_2, R) \tag{16}$$

where

$$FQ_q^{ij}(r_2, R) = \int_{|R-r_2|}^{R+r_2} \mathrm{d}r_1 r_1^q \mathscr{R}_i(r_1)\mathscr{R}_j(r_1). \tag{17}$$

These last integrals can be performed analytically (to yield products of polynomials with exponential functions) for radial wavefunctions of the type described in §1.2. The final integration (over the variable r_2) is of the same sort and yields formulae for the $B_{U_k}^{(L,S)}(|R)$ involving polynomials, exponentials and integral logarithms of R.

To evaluate the matrix elements of G we have used a (presumably) rapidly converging expansion proposed by Baylis:

$$B_G^{(L,1)}(i,j|R) = \left(\frac{2L+1}{4\pi}\right)^{1/2} (3\pi^2)^{2/3} Z_B^{2/3} \left[I_1 \Delta_{i,j} + I_3 \frac{1}{6R^2} \left(-L(L+1) + 2R\frac{\mathrm{d}}{\mathrm{d}R} + R^2 \frac{\mathrm{d}^2}{\mathrm{d}R^2} \right) \mathscr{R}_i(R)\mathscr{R}_j(R) + \ldots \right] \tag{18}$$

with

$$\Delta_{ij} = \int_0^\infty \mathrm{d}r_1 r_1^2 \mathscr{R}_i(r_1)\mathscr{R}_j(r_1)$$

and

$$I_S = \int_0^\infty \mathrm{d}r_2 r_2^{S-1} [\rho_B(r_2)/Z_B]^{2/3}.$$

The relationships displayed here provide the means for evaluating the matrix elements of U_I analytically. The procedure is algebraically complex and tedious to program but it is inexpensive to run.

3. Matrix elements for Li–He and Li–Ne

3.1. Numerical evaluation

The numerical integration procedure of §2.1 has been used to evaluate the matrix elements, $U_{jj'}^{(\mathrm{BODY})}(R)$, of the two systems Li–He and Li–Ne associated with the 2s, $2p_0$ and $2p_1$ states of Li. Calculations for Na–He/Ne have also been performed but are not reported here. To simplify the notation we introduce for these three states the labels $j = 1$, 2 and 3, respectively. For both systems calculations were made using the two different values of the potential parameter, r_0, generated by Baylis and by Pascale and Vandeplanque, viz for Li–He, $r_0 = 0{\cdot}885$ au and $1{\cdot}030$ au and for Li–Ne, $r_0 = 1{\cdot}037$ au and $1{\cdot}207$ au.

It is convenient to separate from U_I, and so then to group with $W(R)$, the potential contribution $V_c(R) = -\alpha_B/2R^4$ which results from polarization of the rare-gas atom by the (point charge) core of the Li^+ ion. The two terms, $W(R)$ and $V_c(R)$, contribute nothing to the off-diagonal elements and add in a simple way to give the diagonal elements V_{jj} of the complete interaction $V_I(\boldsymbol{r}_1, \boldsymbol{R})$. Accordingly, we define the reduced model potential

$$U_B \equiv U_I(\boldsymbol{r}_2, \boldsymbol{R}) - V_c(R) = G(r_2) + V_e(r_2) + V_{ec}(\boldsymbol{r}_2, \boldsymbol{R}) \tag{19}$$

consisting of the sum of the repulsive exchange interaction, G, the electron polarization term V_e, and the electron–core cross polarization term V_{ec} of the induction potential, $F(r_2, R)$, cf equations (2,.3). We present here values of the matrix elements,

$$U_{jj'}(R) = U_{jj'}^{(\mathrm{BODY})}(R) - V_c(R)\,\delta_{jj'} = U_{jj'}^{(\mathrm{BODY})}(R) + \frac{\alpha_B}{2R^4}\,\delta_{jj'} \tag{20}$$

of the reduced Baylis model potential U_B. In figures 3(*a*)–(*d*) we display the R dependence of the four independent matrix elements U_{11}, U_{22}, U_{33} and U_{12} for the system

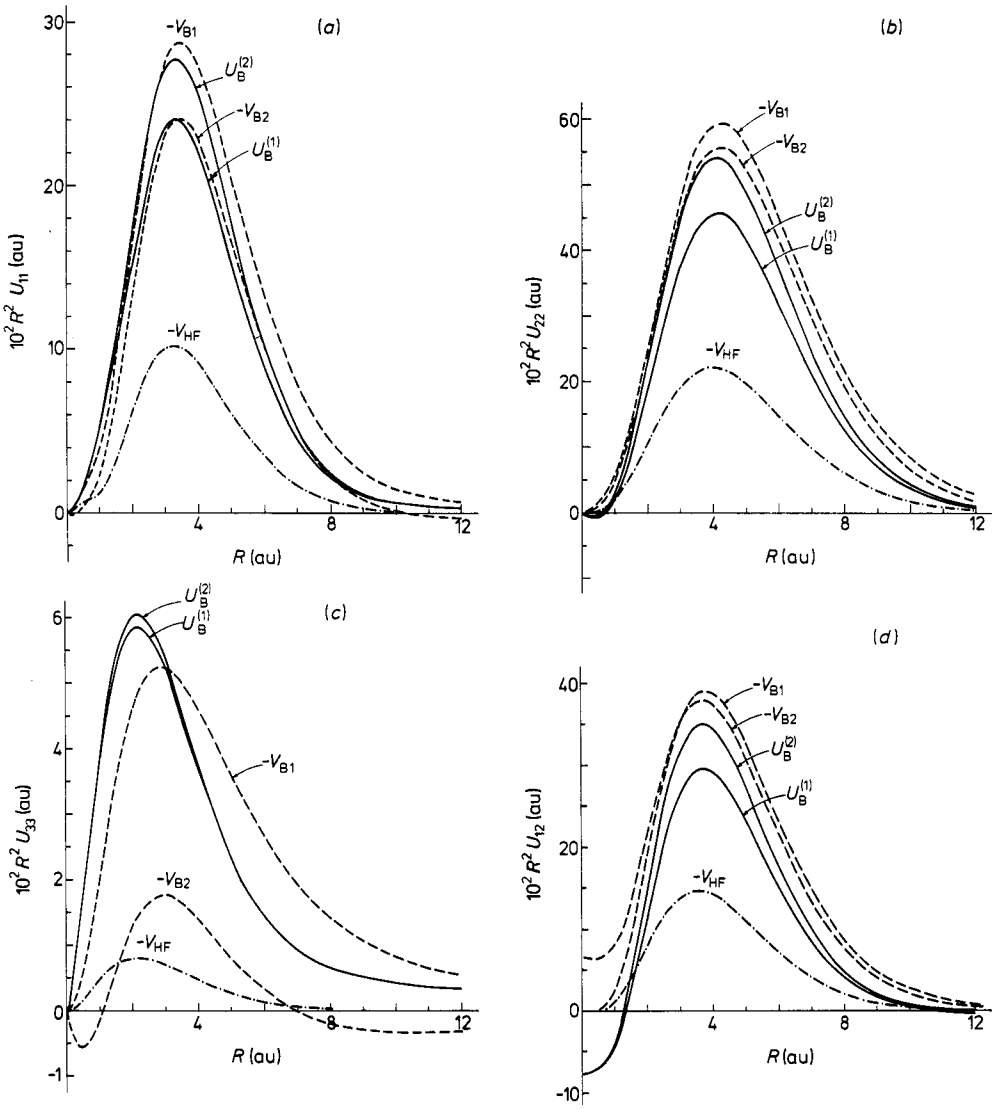

Figure 3. Matrix elements $U_{jj'}^{(\mathrm{BODY})}(R)$ for the Li–He system based upon the model potentials U_B, $-V_{HF}$, $-V_{B1}$ and $-V_{B2}$. $U_B(r_2, R)$ is the reduced Baylis potential, equation (19), for $r_0 = 0{\cdot}885$ au ($U_B^{(1)}$) and for $r_0 = 1{\cdot}030$ au ($U_B^{(2)}$). $V_{HF}(r_2)$ is the Hartree–Fock frozen-core potential, equation (21), and $V_{B1}(r_2)$ and $V_{B2}(r_2, R)$ are the Bottcher potentials, equations (22)–(23). Notice that we have chosen to plot $R^2U_{jj'}(R)$ against R, the internuclear distance. The matrix elements shown are: (*a*)–(*c*) the three diagonal elements U_{11}, U_{22}, U_{33} (2s–2s, $2p_0$–$2p_0$ and $2p_1$–$2p_1$, respectively) and (*d*) the off-diagonal element U_{12} (2s–$2p_0$).

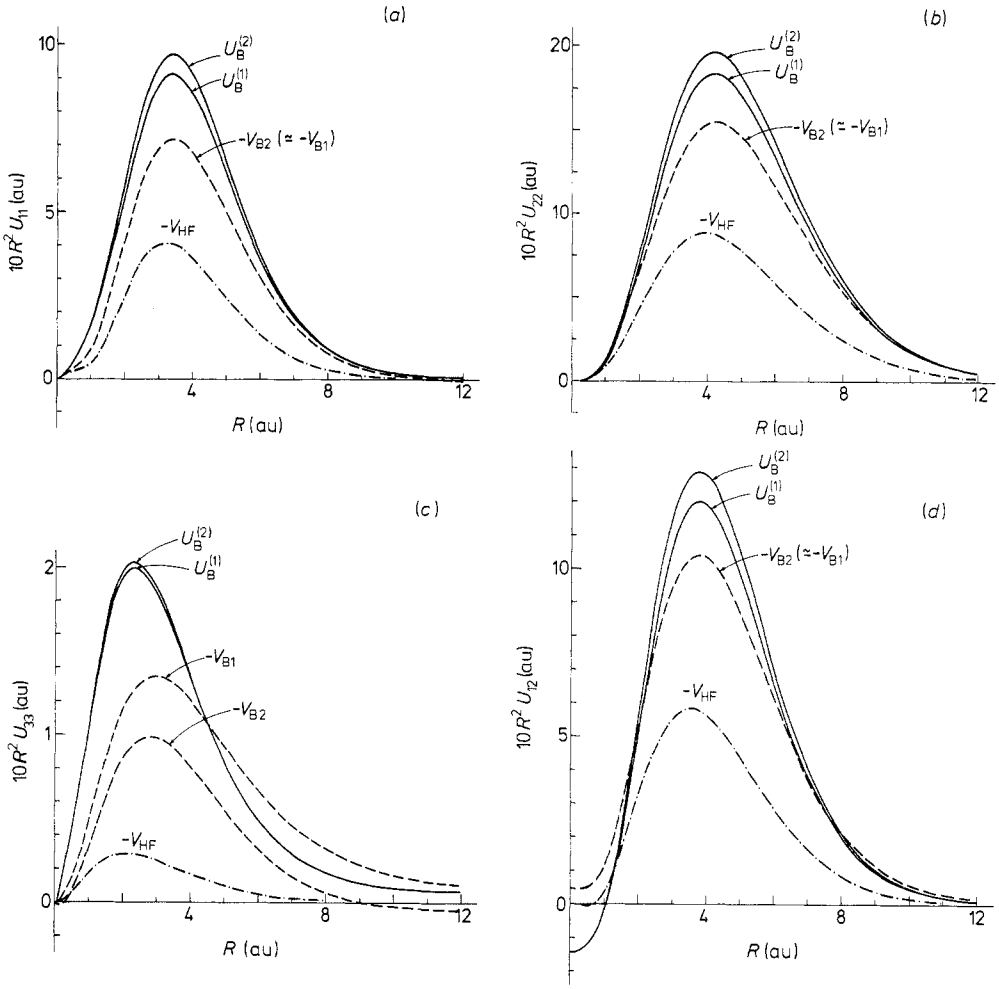

Figure 4. Matrix elements $U_{jj'}^{(\mathrm{BODY})}(R)$ for the Li–Ne system based upon the model potentials U_B, $-V_{HF}$, $-V_{B1}$ and $-V_{B2}$. $U_B(r_2, \boldsymbol{R})$ is the reduced Baylis potential, equation (19), for $r_0 = 1{\cdot}037$ au ($U_B^{(1)}$) and for $r_0 = 1{\cdot}207$ au ($U_B^{(2)}$). $V_{HF}(r_2)$ is the Hartree–Fock frozen-core potential, equation (21), and $V_{B1}(r_2)$ and $V_{B2}(r_2, \boldsymbol{R})$ are the Bottcher potentials, equations (22)–(23). Notice that we have chosen to plot $R^2 U_{jj'}(R)$ against R, the internuclear distance. The matrix elements shown are: (*a*)–(*c*) the three diagonal elements U_{11}, U_{22}, U_{33} (2s–2s, $2p_0$–$2p_0$ and $2p_1$–$2p_1$, respectively) and (*d*) the off-diagonal element U_{12} (2s–$2p_0$).

Li–He and for particle separations of importance in inelastic collisions. Corresponding matrix elements for the system Li–Ne are shown in figures 4(*a*)–(*d*). Also included in figures 3 and 4 are matrix elements associated with other model potentials for the Li–He/Ne systems. These are discussed in §4.

Actually, what we have plotted in these figures are values of the functions $R^2 U_{jj'}(R)$. Because of the singular behaviour of the electron–core cross polarization potential, $V_{ec} = -\alpha_B \cos\theta_2 / R^2 r_2^2$, the off-diagonal element behaves in the manner $U_{12}(R) \rightarrow -R^{-2}$ as $R \rightarrow 0$. To specify more clearly the behaviour of the diagonal and off-diagonal matrix elements in the limits $R \rightarrow 0$ and $R \rightarrow \infty$, we have collected in table 1 information about the Baylis potential and about the other model

Table 1. The limiting behaviour ($R \to 0$ and $R \to \infty$) of diagonal and off-diagonal matrix elements $U_{jj'}^{(\mathrm{BODY})}(R)$ (for the Li–He system: $j = 1(2s)$, $j = 2(2p_0)$, $j = 3(2p_1)$) using the Hartree–Fock frozen-core potential V_{HF}, the Bottcher potentials $V_{\mathrm{B}1}$ and $V_{\mathrm{B}2}$, equations (21)–(23), and the reduced Baylis potential U_{B}, equation (19).

Matrix element	Model potential	$R \to 0$	$R \to \infty$
$U_{jj}(R)$	V_{HF}	$\sim R^0$	$\sim -\mathrm{e}^{-\beta R}$
	$V_{\mathrm{B}1}$	$\sim R^0$	$\sim -\alpha_{\mathrm{B}}/2R^4$
	$V_{\mathrm{B}2}$	$\sim R^{-1}$	$\sim +\alpha_{\mathrm{B}}/2R^4$
	U_{B}	$\sim R^0$ $(j = 1)$	$\sim +\alpha_{\mathrm{B}}/2R^4$
		$\sim R^{-1}$ $(j = 2, 3)$	
$U_{12}(R)$	V_{HF}	$\sim R$	$\sim -\mathrm{e}^{-\beta R}$
	$V_{\mathrm{B}1}$	$\sim R$	$\sim -R^{-5}$
	$V_{\mathrm{B}2}$	$\sim -R^{-2}$	$\sim -R^{-7}$
	U_{B}	$\sim -R^{-2}$	$\sim -R^{-7}$

interactions as well. In the limit $R \to 0$ the diagonal elements $U_{jj}(R)$ of the Baylis potential go as R^0 for $j = 1(2s)$, due to the terms G and V_{e}, and as R^{-1} for $j = 2, 3$ ($2p_0$ and $2p_1$), due to the term V_{ec}. As $R \to \infty$ all diagonal elements are dominated by the term $+\alpha_{\mathrm{B}}/2R^4$ which comes from V_{e} and V_{ec} (and hence $V_{jj} \to -R^{-6}$, the asymptotically correct van der Waals interaction). For this same reason the asymptotic form of the off-diagonal element is given by $U_{12} \to -R^{-7}$. Over the intermediate range, $1{\cdot}5 \leqslant R \leqslant 8$ au, the repulsive term G dominates the diagonal and off-diagonal elements, all of which are positive valued and exhibit maxima within this range of R values. Matrix elements for Li–Ne generally are about three times as large as the corresponding matrix elements for the system Li–He.

For the Li–He system the two values of r_0 (0·885 and 1·030 au) result in matrix elements $U_{jj'}(R)$ very similar in shape (cf figures 3(*a*)–(*d*)) and differing in magnitude by no more than 15% (for U_{33} the difference is only about 2%) throughout the complete range of separations, $0 \leqslant R \leqslant 8$ au. In the case of Li–Ne (cf figures 4(*a*)–(*d*)) there is even less sensitivity to the choice for r_0 (1·037 and 1·207 au). This lack of sensitivity is consistent with the weak r_0 dependence of the well depth reported by both Baylis and by Pascale and Vandeplanque.

In figure 5 we present the short-range Pauli-exclusion pseudopotential, $W(R)$, for the repulsion between the alkali core and the rare-gas atom for Li–He and Li–Ne. These were calculated directly from equations (5)–(6) using the numerical integration procedure described in §2.1. Baylis and Pascale and Vandeplanque did not attempt to calculate this function exactly. Their procedures for estimating the value of $W(R)$ involve a number of mathematical approximations, the adequacies of which are difficult to determine without numerical experimentation. We note that $W(R)$ tends to a positive constant in the limit $R \to 0$ and that it falls rapidly to zero for $R > 2$ au.

3.2. Analytical evaluation

Using the analytical procedure described in §2.2, we have evaluated the contributions from F and G separately (cf equations (1)–(4)) to the matrix elements of the Baylis interaction. Results for the 2s–2s and 2s–$2p_0$ matrix elements are presented in table 2 along with the corresponding results obtained by the numerical integration

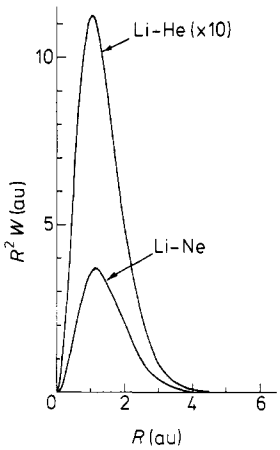

Figure 5. The short-range Pauli-exclusion pseudopotential $W(R)$, equations (5)–(6), for the repulsion between the alkali ion core and the rare-gas atom for Li–He and for Li–Ne. Note that the $W(R)$ values for Li–He has been multiplied by 10.

procedure. The perfect agreement (to about six decimals) between F_{ij}^{anal} and F_{ij}^{num} testifies to the high accuracy of the numerical double integration. The values of G_{ij}^{anal} and G_{ij}^{num} are very nearly equal as R grows large but differ greatly as R approaches zero. These differences are due to the failure at small R of the expansion which led to the (truncated) series representation, equation (18), for G. It is only for $R > 2{\cdot}5$ au that the analytic approximation to the matrix elements of G agrees to within 6% with the results of the 'exact' numerical integration. When programmed for computation the analytical procedure is much faster and more economical than the numerical integration. However, the matrix elements of G for the intermediate range $1 \leqslant R \leqslant 3$ au do play a significant role in the theory of high-energy inelastic collisions. To calculate these with accuracy it is necessary to use the exact numerical scheme. Pascale and Vandeplanque report that the approximate approach is fairly accurate for the range of intermediate and large internuclear separations but give no details.

4. Comparison with other model potentials

In this section we shall present matrix elements for Li–He and Li–Ne obtained from several quite different model potentials.

A simplistic approach, widely used in the study of inelastic collisions between hydrogen atoms with rare-gas atoms, is to assume a Coulombic interaction between the hydrogenic electron and the undisturbed, 'frozen-core' charge distribution of the rare-gas atom. Various approximations can be used for the electron density of this atom. We choose the Hartree–Fock approximation and so obtain the potential

$$V_{\text{HF}}(r_2) = 2\sum_{nlm}\int \mathrm{d}^3 r\, \frac{|\phi_{nlm}(\boldsymbol{r})|^2}{|\boldsymbol{r}_2 - \boldsymbol{r}|} - 2\sum_{nl}\frac{2l+1}{r_2}$$

$$= -\frac{2}{r_2}\sum_{nl}(2l+1)\int_{r_2}^{\infty}\mathrm{d}r\, r^2 \mathscr{R}_{nl}^2(r)(1 - r_2/r) \tag{21}$$

where the functions $\phi_{nlm}(\boldsymbol{r}) = \mathscr{R}_{nl}(r)Y_{lm}(\hat{r})$ are the SCF orbitals of the closed-shell rare-gas atom (Clementi 1965).

The assumption that the electron-dependent part of the alkali–rare-gas interaction is given by $V_A(r_1) + V_{HF}(r_2)$ amounts to a total neglect of the distortional effects due to the presence of the electron and of the alkali core, that is, of the polarization potential $F(\boldsymbol{r}_2, \boldsymbol{R})$ of the Baylis model. (Also neglected by this approximation are the Pauli exclusion forces.) Bottcher (1971) and Bottcher *et al* (1973) have improved the HF frozen-core, electron–rare-gas potential by replacing V_{HF} with

$$V_{B1}(r_2) = V_{HF}(r_2) + V_e(r_2)\, w_6(r_2) + V_q(r_2)\, w_8(r_2) + V_{sr}(r_2). \tag{22}$$

Here V_e and V_q are the induced dipole and quadrupole interactions. Each is multiplied by an extremely short ranged cut-off function, w_6 or w_8, which eliminates the divergence of the potential at $r_2 = 0$. V_{sr} is a short-range, exponentially varying potential, the parameters of which are adjusted in order to fit the experimental electron–rare-gas momentum-transfer cross section. We have chosen to use V_{B1} parameters of Bottcher *et al* (1973).

The assumption that $V_A(r_1) + V_{B1}(r_2)$ is the electron-dependent part of the alkali–rare-gas interaction corresponds to a neglect of the cross polarization term $V_{ec}(\boldsymbol{r}_2, \boldsymbol{R})$. This potential, $V_A + V_{B1}$, has been used by Nielsen and Dahler (1976) in previous studies of inelastic alkaline-earth-ion–rare-gas-atom collisions. Bottcher *et al* (1973) have included the electron–alkali-core cross polarization potential, $V_{ec}(\boldsymbol{r}_2, \boldsymbol{R})$, as a perturbation to the molecular Hamiltonian in order to get the proper long-range van der Waals' interactions. Therefore, it is both natural and convenient to introduce the potential

$$V_{B2}(\boldsymbol{r}_2, \boldsymbol{R}) = V_{B1}(r_2) + V_{ec}(\boldsymbol{r}_2, \boldsymbol{R}) \tag{23}$$

in which case the electron-dependent part of the model potential is given by $V_A(r_1) + V_{B2}(\boldsymbol{r}_2, \boldsymbol{R})$.

To compare these four model potentials more systematically retaining only the r_2-dependent terms) we write

$$U_B = G + V_e\eta(r_2 - r_0) + V_e(r_0)\eta(r_0 - r_2) + V_{ec}\eta(r_2 - r_0) \tag{24}$$

$$V_{B1} = (V_{HF} + V_{sr}) + V_e w_6 + V_q w_8 \tag{25}$$

$$V_{B2} = (V_{HF} + V_{sr}) + V_e w_6 + V_q w_8 + V_{ec} w_4 \tag{26}$$

where $\eta(x)$ is the unit step function. In the Baylis potential, U_B of equation (24), the divergencies at $r_2 = 0$ are taken care of by the introduction of a sphere of radius r_0 inside of which $V_e(r_2) = V_e(r_0)$ and $V_{ec} = 0$, cf equations (2) and (3). In the Bottcher potentials, V_{Bj}, the divergencies are removed by the insertion of cut-off factors w_n, with the properties $w_n \simeq 1$ for $r_2 > r_0$ and $w_n \to r_2^n$ for $r_2 \to 0$. The values of the parameter r_0 differ only slightly in the Baylis and Bottcher models.

The actual evaluation of the matrix elements $U_{jj'}$ based upon V_{HF}, V_{B1} and V_{B2} follows in part the analytic scheme discussed in §2.2. However, the final integration (over the variable r_2) was done numerically, as previously reported for V_{B1} by Nielsen and Dahler (1976).

We have chosen in figures 3–4 to plot the matrix elements U_{ij} of the three potentials $-V_{HF}$, $-V_{B1}$ and $-V_{B2}$ along with the corresponding elements of the Baylis potentials U_B. This has been done because of the strikingly similar shapes

Table 2. Comparison of matrix elements of the Baylis potential components F, equations (2)–(3), and G, equation (4), when evaluated by the analytical procedure, §2.2, and by the numerical procedure, §2.3.

	$\langle 2s\|F\|2s\rangle$		$\langle 2s\|G\|2s\rangle$		
R	Analytical	Numerical	Analytical	Numerical	$G_{11}^{anal}/G_{11}^{num}$
0·1			−5·81814 (1)	1·10242 (−1)	−5·28 (2)
0·25			−4·32273	1·01180 (−1)	−4·27 (1)
0·50			1·24515	8·11998 (−2)	1·53 (1)
0·75			5·99012 (−1)	6·65132 (−2)	9·01
1·0	−7·02616 (−1)	−7·02618 (−1)	1·82379 (−1)	5·99248 (−2)	3·04
1·5			2·66566 (−2)	5·96323 (−2)	4·47 (−1)
2·0	−5·92376 (−2)	−5·92376 (−2)	4·36666 (−2)	5·94548 (−2)	7·34 (−1)
2·5			5·01639 (−2)	5·33573 (−2)	9·40 (−1)
3·0	−2·19136 (−2)	−2·19136 (−2)	4·40494 (−2)	4·35041 (−2)	1·013
3·5			3·40890 (−2)	3·29816 (−2)	1·034
4·0	−1·04788 (−2)	−1·04788 (−2)	2·45359 (−2)	2·36688 (−2)	1·037
5·0	−4·84374 (−3)	−4·84374 (−3)	1·10861 (−2)	1·08120 (−2)	1·025
6·0	−2·11038 (−3)	−2·11038 (−3)	4·42537 (−3)	4·39997 (−3)	1·006
7·0	−8·81834 (−4)	−8·81833 (−4)	1·62108 (−3)	1·64773 (−3)	9·84 (−1)
8·0	−3·62306 (−4)	−3·62306 (−4)	5·57897 (−4)	5·79700 (−4)	9·62 (−1)

	$\langle 2s\|F\|2p_0\rangle$		$\langle 2s\|G\|2p_0\rangle$		
R	Analytical	Numerical	Analytical	Numerical	$G_{12}^{anal}/G_{12}^{num}$
0·1			5·13934	1·71569 (−3)	3·00 (3)
0·25			2·55322	5·06400 (−3)	5·04 (2)
0·50			7·19000 (−1)	1·41035 (−2)	5·10 (1)
0·75			1·54946 (−1)	2·67997 (−2)	5·78
1·0	−7·67507 (−2)	−7·67509 (−2)	1·41949 (−2)	4·05453 (−2)	3·50 (−1)
1·5			2·15553 (−2)	6·20917 (−2)	3·47 (−1)
2·0	−3·38880 (−2)	−3·38882 (−2)	5·46415 (−2)	7·02135 (−2)	7·78 (−1)
2·5			6·31012 (−2)	6·71035 (−2)	9·40 (−1)
3·0	−2·27625 (−2)	−2·27625 (−2)	5·76792 (−2)	5·77923 (−2)	9·98 (−1)
3·5			4·72886 (−2)	4·63904 (−2)	1·019
4·0	−1·37819 (−2)	−1·37819 (−2)	3·63294 (−2)	3·53792 (−2)	1·027
5·0	−7·43907 (−3)	−7·43908 (−3)	1·89030 (−2)	1·84252 (−2)	1·026
6·0	−3·68560 (−3)	−3·68560 (−3)	8·77272 (−3)	8·63231 (−3)	1·016
7·0	−1·71931 (−3)	−1·71931 (−3)	3·76345 (−3)	3·74992 (−3)	1·004
8·0	−7·70951 (−4)	−7·70951 (−4)	1·52524 (−4)	1·53970 (−4)	9·91 (−1)

and magnitudes of these matrix elements for the important intermediate range of R values. On the other hand, when the concern is with the limits $R \to 0$ and $R \to \infty$ it is preferable to compare the matrix elements of V_{HF}, V_{B1}, V_{B2} and U_B, as has been done in table 2.

In the limit $R \to \infty$ and r_1 finite ($r_2 \to R$) the physical bases of the potentials U_B and V_{B2} are much the same (compare equations (24) and (26)) and their matrix elements behave similarly, cf §3.1. However, in this same limit the matrix elements of U_{B1} are dominated by V_e and so U_{jj} falls off asymptotically, and incorrectly, as $-R^{-4}$. The short-range potential V_{HF} results in matrix elements that decay exponentially at large internuclear separations.

The matrix elements of U_B and V_{B2} diverge as R approaches zero because of the singularity at the origin of the cross polarization potential, $V_{cc} \rightarrow -R^{-2}$. The exception to this statement is the U_{11} element of U_B which varies as R^0 because of the different ways in which the Bottcher and Baylis potentials deal with the singularities at $r_2 = 0$. For this same reason the limiting values of R^2U_{12} at $R = 0$ are slightly different for U_B and V_{B2}. The matrix elements of V_{HF} and V_{B1} behave similarly to one another as $R \rightarrow 0$: only the short-range part of V_{B1} contributes in this limit.

In the intermediate range $1{\cdot}5 \leqslant R \leqslant 8$ au the matrix elements of V_{B1} and V_{B2} differ only slightly. For these separations the principle effect of the cross polarization potential is to lower the magnitudes of U_{11}, U_{22} and U_{12}—by no more than 15% for Li–He, cf figures 3(*a*)–(*d*), and by less than 1% in the case of Li–Ne, an effect which is too small to be detected in figures 4(*a*)–(*d*). It is obvious from figures 3(*c*) and 4(*c*) that the differences are far greater for U_{33} but this matrix element is an order of magnitude smaller than the others and so of little importance in the calculation of collision cross sections. These results suggest that there may be situations where the use of V_{B1} in place of the more complicated V_{B2} is well justified. In the following paper (Manique *et al* 1977) we shall examine this possibility on a quantitative basis by calculating cross sections for several inelastic alkali–rare-gas collisional events using both of these model potentials. In an earlier calculation of the quenching cross section for H(2s) by He, Byron and Gersten (1971) found that the $2s$–$2p_0$ matrix elements of the cross polarization potential could be neglected throughout the relevant range of internuclear separations.

Use of the very simple frozen-core electrostatic interaction V_{HF} results in matrix elements which are significantly smaller at intermediate ranges than those obtained from V_{B1}, V_{B2} and U_B. The Hartree–Fock values are typically 30% of the others for Li–He and 50% for Li–Ne. Although the shapes of the V_{HF} matrix elements are much the same as the others, the half-widths of the bell-shaped functions $U_{ij}(R)$ are significantly smaller. This results from the absence in V_{HF} of long-range polarization terms.

The physical basis of the Baylis model potential U_B is very different from that of the simple Hartree–Fock potential V_{HF} and from that of the two Bottcher potentials, V_{B1} and V_{B2}, as well. The short-range part of U_B includes the repulsive Pauli-exclusion potential, $G(r_2)$, in contrast to the short-range attractive electrostatic fields V_{HF} and $V_{HF} + V_{sr}$ of V_{B1} and V_{B2}, respectively. However, the magnitudes of the matrix elements of V_{B1}, V_{B2} and U_B are surprisingly similar for all the states of Li–He and Li–Ne that we have investigated. However the algebraic signs of the V_{Bj} and U_B matrix elements are different over the entire intermediate range of internuclear distances. The common R dependence of these matrix elements can be understood in terms of their strong dependence upon the overlap of the wavefunctions of the alkali valence electron. Matrix elements which differ only in algebraic sign produce excitation cross sections that are equal to first order.

5. Concluding remarks

We have seen that the matrix elements of the Baylis model potential for Li–rare-gas systems are fairly sensitive to the choice of the cut-off parameter in the case of He but distinctly less so in the case of Ne. The values of r_0 for these systems suggested by Baylis and by Pascale and Vandeplanque were not obtained by fitting

Table 3. Ground-state well depths ϵ_0 and internuclear equilibrium distances R_0 for alkali–rare-gas diatoms obtained from recent experiments (Dehmer and Wharton 1972, Carter *et al* 1975), compared to the results implied by the model potentials of Baylis (1969) and of Pascale and Vandeplanque (1974) (U_B for two different choices of r_0) and to the predictions by the model potential of Bottcher (Bottcher *et al* 1973).

	Experiment		Baylis		Pascale and Vandeplanque		Bottcher	
System	R_0(au)	ϵ_0(cm^{-1})	R_0(au)	ϵ_0(cm^{-1})	R_0(au)	ϵ_0(cm^{-1})	R_0(au)	ϵ_0(cm^{-1})
Li–He	11·3–12	0·81–1·12	10·6	2·0	11·25	2·1	12	1·0
Li–Ne	9·3–9·6	8·80–9·61	12·5	1·5	12·65	2·0	10	3·3
Na–Ne	9·1	11	12·9	1·3	13	1·8	12	3·8

to experimental values of the ground-state well depth ϵ_0 but by extrapolation from a correlation of r_0 with $\langle r^2 \rangle^{1/2}$ which was developed from data available for alkali diatoms and the heavier rare gases, Ar, Kr and Xe. Experimental values of ϵ_0 that were recently reported (Dehmer and Wharton 1972) for the Li–He/Ne systems and for Na–Ne (Carter *et al* 1975) differ significantly from those calculated from the Baylis potentials based upon extrapolated estimates for the r_0 parameters, cf table 3. The well depths for Li–He obtained from measurements of elastic cross sections range from 0·81 cm^{-1} to 1·12 cm^{-1} (depending on details of the analytic fitting procedure) and occur at separations of R_0 = 11·3–12 au. For this system Baylis obtains a well depth of 2·0 cm^{-1} (for r_0 = 0·885 au) at R_0 = 10·6 au and Pascale and Vandeplanque get ϵ_0 = 2·1 cm^{-1} (for r_0 = 1·030 au) at R_0 = 11·25 au. The scattering experiments for Li–Ne yield a well depth in the range 8·80–9·61 cm^{-1} and R_0 between 9·3 and 9·6 au. In this case Baylis obtains 1·5 cm^{-1} (for r_0 = 1·037 au) at R_0 = 12·5 au and Pascale and Vandeplanque get 2·0 cm^{-1} (for r_0 = 1·207 au) at R_0 = 12·65 au.

The well depths of the Baylis potential do not appear to depend sensitively upon the value of r_0 and Pascale and Vandeplanque's values for this parameter do not produce well depths that are in significantly better agreement with experiment than those generated by Baylis' choices for this parameter. The ground-state well depths for Li–He/Ne that result from Bottcher's model potential do correlate somewhat better with the experimental results. Thus, Bottcher *et al* (1973) report ϵ_0 = 1·0 cm^{-1} and R_0 = 12 au for Li–He and ϵ_0 = 3·3 cm^{-1} and R_0 = 10 au for Li–Ne. The same conclusions may be drawn for the Na–Ne results presented in table 3.

Although the physical basis of the Baylis potential may appear to be more sound than that of the Bottcher potential, the single parameter r_0 and its correlation with the ground-state well depth does not seem to be sufficiently flexible. This is particularly apparent in connection with the r_0-extrapolation procedure, for which the resulting agreement with experimental well depths is not at all satisfactory. However, it is distinctly possible that this emphasis upon the very shallow wells of the alkali–rare-gas potentials (and so upon the long-range attractive parts of the complete interaction V_I) is misplaced, especially when the main concern is with potentials to be used in high-energy collisions.

We have considered in detail the matrix elements, U_{ij}, of the electron-dependent parts of the Baylis model potential, U_B, and of the Bottcher and Hartree–Fock potentials V_{B1}, V_{B2} and V_{HF}. The matrix elements of U_B were found to depend fairly sensitively upon the choice of the cut-off parameter, r_0, and to differ markedly from

the corresponding matrix elements of the Bottcher and Hartree–Fock potentials. Much of the physics of inelastic alkali–rare-gas collisions is contained within these matrix elements. In the accompanying paper we use these in a semiclassical impact-parameter theory to compute the total cross sections for inelastic collisions.

Acknowledgments

This work has in part been supported by a grant from the National Science Foundation. One of us (SEN) wishes to acknowledge a grant from the Danish Natural Science Research Council, and to express his gratitude for the hospitality extended to him during his visit to the University of Minnesota.

References

Baylis W E 1969 *J. Chem. Phys.* **51** 2665–79
Bottcher C 1971 *J. Phys. B: Atom. Molec. Phys.* **4** 1140–9
Bottcher C, Dalgarno A and Wright E L 1973 *Phys. Rev.* A **7** 1606–9
Byron F W and Gersten J I 1971 *Phys. Rev.* A **3** 620–34
Carter G M, Prichard D E, Kaplan M and Ducas T W 1975 *Phys. Rev. Lett.* **35** 1144–6
Clementi E 1965 *IBM J. Res. Dev.* **9** 2–19
Dehmer P and Wharton L 1972 *J. Chem. Phys.* **57** 4821–35
McLean A D and Yoshimine M 1965 *IBM J. Res. Dev.* **9** 203–4
Manique J. Nielsen S E and Dahler J S 1977 *J. Phys. B: Atom. Molec. Phys.* **10** 1703–22
Messiah A 1961 *Quantum Mechanics* (New York: Interscience) Appendix C IV
Nielsen S E and Dahler J S 1976 *J. Phys. B: Atom. Molec. Phys.* **9** 1383–99
Pascale J and Vandeplanque J 1974 *J. Chem. Phys.* **60** 2278–89
Rapp D and Chang C 1972 *J. Chem. Phys.* **57** 4283–6
——1973 *J. Chem. Phys.* **58** 2657
Schaefer H F III 1970 *J. Chem. Phys.* **52** 6241–7